ACS Photonics

Letter

pubs.acs.org/journal/apchd5

Contributions of Correlated Acentric Atomic Displacements to the Nonlinear Second Harmonic Generation and Response

Antonio Cammarata and James M. Rondinelli*

Department of Materials Science and Engineering, Drexel University, 3141 Chestnut Street, Philadelphia, Pennsylvania 19104-2816, United States

ABSTRACT: Group theory and ab initio electronic structure calculations are combined to formulate a general protocol called "SAFOR" to understand and predict how to improve the second harmonic generation (SHG) response in acentric nonlinear optical crystals. Using the prototypical SHG borate β-BaB_2O_4, we show how the SHG d-tensor can be formulated from mode effective d_{ij} coefficients obtained as a linear combination of symmetry-adapted displacement patterns that transform as irreducible representations of a centrosymmetric parent structure. Since this protocol does not require any constraints on the crystal topology or anionic moieties in the structure, we suggest it constitutes a powerful tool to understand and design new SHG compounds through atomic-structure governing principles.

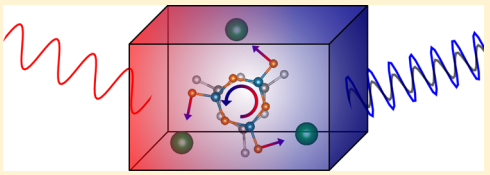

KEYWORDS: *non-linear optics, second harmonic generation, borates, group theory*

Tunable laser frequency sources are required in a variety of applications ranging from the study of correlated electrons in superconductors,[1] interfacial electrochemical energy conversion reactions,[2] materials processing,[3] medical imaging technologies,[4] and building secure high-speed optical networks.[5] They often rely on frequency-doubled light, achieved through a nonlinear optical (NLO) light−matter interaction known as second-harmonic generation (SHG) that is active in materials without inversion symmetry.[6] The absence of inversion symmetry is a necessary condition, but depending on the physio-chemical properties, for example, birefringence, phase-matchability,[7] transparency (absorption) edges, mechanical strength, and critically high SHG coefficients (d_{ij}), strong performance is not guaranteed. Therefore, the relationship between the atomic structural features and the macroscopic optical coefficients should be explored to understand how to design and discover high-performing SHG crystals.

Experimental discovery of new and useful NLO crystals with large SHG coefficients is challenging and time-consuming, because it requires development cycles that include candidate material identification, single crystal growth, optical testing, and further structural optimization.[8] Several computational methods have been developed to make the process more efficient by narrowing the composition−structure phase space for experimental exploration to only the most favorable structures and chemistries. Chen's well-established "anionic group theory" provides a fast computational method to aid the search of new NLO crystals,[9,10] however, it relies on a priori understanding that well-defined anionic groups exists in the structure, a major limitation when the structure lacks well-defined polyhedral units as in many low-dimensional structures containing 1D chains.[11]

An alternative method called the real-space-atom-cutting (RSAC) approach is based on the decomposition of the electronic density into atomic contributions.[12−14] It has proven useful in explaining how chemical substitution can enhance SHG in established structure types,[15] because unlike Chen's method, it is able to distinguish among the single atomic contributions rather than collective anionic moieties to the global SHG response. Yet, there is no unique way to partition the electronic charge density in crystalline materials, and the RSAC method requires substantial testing of different partitioning schemes. It largely benefits from a thorough electronic structure understanding of the NLO crystal, features problematic when searching for or designing new compounds in advance of synthesis.

Recently, we introduced a symmetry-based approach[16] to quantify the degree of inversion symmetry breaking in a polar structure. The authors of ref 16 showed that it is possible to correlate the observed macroscopic SHG intensity with the amplitude, specifically of collective displacement modes, and "density" of polar distortions. This description, however, did not formally establish a connection between such displacements and the size of the second-order dielectric susceptibility.

Building from this last approach, we show in this Letter that the SHG response (d_{ij} tensor) can be decomposed into unique acentric structural contributions using a Symmetry-Assisted Functional Optical Response (SAFOR) analysis, which unites applied group theory and ab initio density functional calculations to understand the origin of the magnitudes of the SHG coefficients. We formulate an atomic structure−optical function relationship in terms of a response activated at a symmetry breaking transition due to correlated atomic displacements, in a similar manner done previously for the electric polarization and Curie temperature in ferroelectric materials.[17] We apply the SAFOR formalism to the widely used

Received: September 20, 2013
Published: January 8, 2014

   dx.doi.org/10.1021/ph400049h | *ACS Photonics* 2014, 1, 96−100

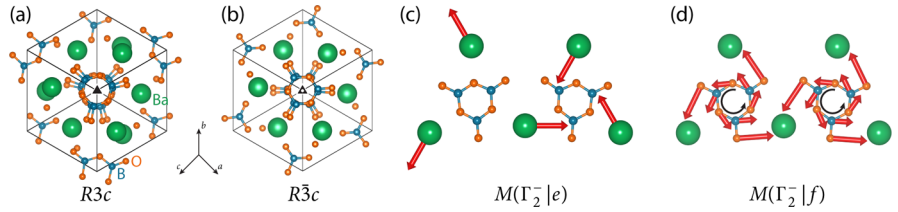

Figure 1. Polar SHG-active (a) and pseudosymmetric (b) BaB_2O_4 structures. The inversion center is absent in the polar phase owing to the $M(\Gamma_2^-|e)$ mode describing Ba^{2+} displacements (c), and $M(\Gamma_2^-|f)$ characterizing the rotation of $[B_3O_6]^{3-}$ rings (d) about the 3-fold axis.

ultraviolet NLO crystal β-barium borate, BaB_2O_4, which achieves frequency-doubled wavelengths near 189 nm,[18−20] to unambiguously identify which fundamental atomic motifs, for example, the Ba^{2+} cations and $[B_3O_6]^{3-}$ units, dictate the size of the SHG coefficients. From this knowledge, we argue the SAFOR analysis facilities efforts to enhance the SHG response in new or known materials through selective control over the atomic scale distortions using displacement "directors" that stabilize the targeted acentric geometries.

To isolate the contributions of acentric distortions to the SHG response, we follow an approach commonly used in the crystallographic study of displacive phase transitions referred to as mode-crystallography.[21] In this framework, the "distorted" crystal structure of interest with space group symmetry ($\mathcal{H}$) is described relative to a higher pseudosymmetric structure ($\mathcal{G}$) such that a well-defined group−subgroup relationship, that is, $\mathcal{H} \subset \mathcal{G}$, exists between the two phases. The lower symmetry crystal is described as a superposition of static symmetry breaking structural distortions or modes, which represent cooperative atomic displacements that when "frozen" into the high symmetry structure reproduce the symmetry $\mathcal{H}$ and the exact crystal structure of the distorted phase.

Here, we exploit the fact that the distorted (specifically noncentrosymmetric) structure can be written as a linear combination of orthonormal symmetry-adapted modes from a complete basis set[22] consisting of the irreducible representations (irreps) of the space group $\mathcal{G}$. The global displacement vector $\mathbf{u}(\mu, i)$, which "encodes" the essential atomic structure information, that is, atom positions μ and possible Wyckoff orbit splittings i connecting the high- and low-symmetry structures, is obtained as a linear combination of independent modes formulated from irreps at various wavevectors (τ) with mode symmetries (m) within $\mathcal{G}$ as

$$\mathbf{u}(\mu, i) = \sum_{\tau,m} A_{\tau,m} \boldsymbol{\varepsilon}(\tau, m|\mu, i) \tag{1}$$

The summation occurs for normalized atomic displacement vectors ($\boldsymbol{\varepsilon}$) with transformation properties matching a given basis mode $M(\tau, m)$ and amplitude $A_{\tau,m}$ within the asymmetric unit. A complete discussion of the mode-decomposition approach is given in ref 21. This formalism further enables the total atomic displacement pattern to be separated by Wyckoff orbits k of $\mathcal{G}$ using a linear combination of Wyckoff-position (WP) dependent mode displacements

$$\mathbf{u}(\mu, i) = \sum_{k} A_k \mathbf{e}(k|\mu, i)$$

where $\mathbf{e}(k)$ is a normalized atomic displacement pattern for atoms belonging to a single Wyckoff position. In practice, these are obtained from one or more of the symmetry-adapted modes $M(\tau,m)$ appearing in eq 1.

Each mode in the decomposition can then be used to isolate the type of symmetry element lost or maintained across the hypothetical transition and the degree to which the deviations occur, for example, measured in units of length. Relevant symmetry elements in noncentrosymmetric NLO materials include mirror planes, inversion, and rotoinversion, as described recently in ref 23. In this case, the low symmetry phase is noncentrosymmetric and obtained by at least one mode or a combination of two modes that lift inversion symmetry in the high-symmetry centrosymmetric phase. For the noncentrosymmetric structures that are SHG active, this formalism can be applied to any structure type and crystal class, independent of the atomic building block geometry. It could be particularly powerful for understanding how the atomic scale structure of NCS materials that are not polar and lack discernible dipoles in molecular units, for example, chiral or neither but still NCS structures or chain-like units, support SHG.

Since the NLO properties depend on the unit cell structural features,[6,24] we formulate the following *ansatz* as the basis of the SAFOR framework: The static SHG tensor of a noncentrosymmetric (NCS) structure d_{ij} can be written as a linear combination of effective symmetry-adapted mode $M(\tau,m)$ contributions, that is, $d_{ij}(M_l)$, relating the SHG-active structure to a centrosymmetric (SHG-inactive) phase:

$$d_{ij} \simeq \sum_{l} d_{ij}(M_l^k) \tag{2}$$

where each $d_{ij}(M^k)$ is the SHG tensor of the structure obtained by distorting the pseudosymmetric structure with mode M^k and $\boldsymbol{\varepsilon}(\tau,m)$ displacements. Note that each SHG tensor component is proportional to components of the complete third-rank second-order dielectric tensor. The k superscript indicates that the mode may be further decomposed into WP-dependent displacements, and the sum in eq 2 is performed over all modes (l) required to describe the ground state symmetry.

We evaluate the *ansatz* by performing zero-Kelvin density functional theory (DFT) calculations on BaB_2O_4 within the local density[25] and independent electron approximation, neglecting quasi-particle effects, using density-functional perturbation theory, as implemented in the ABINIT package.[26−29] To achieve high-precision in the relaxed-ion nonlinear dielectric susceptibility, we use a plane-wave cutoff of 800 eV and 5 × 5 × 5 k-point mesh. Norm-conserving pseudopotentials, generated with the Troullier-Martins scheme, are used for all atoms with the following valence electron configuration: $6s^25p^6$ (Ba), $2s^22p$ (B), and $2s^22p^4$ (O).

BaB_2O_4 is characterized by planar anionic $[B_3O_6]^{3-}$ rings stacked along the 3-fold axis with Ba^{2+} cations counterions interleaved between the rings as shown in projection along the trigonal axis Figure 1a. The polar β-phase is found in space group $R3c$, point group $3m$, and we identify a hypothetical pseudosymmetric phase with symmetry $R\bar{3}c$ ($\bar{3}m$) (Table 1,

dx.doi.org/10.1021/ph400049h | ACS Photonics 2014, 1, 96−100

Table 1. Crystallographic Parameters for the Hypothetical Centrosymmetric ($R\bar{3}c$) and Polar ($R3c$) BBO Structures Given in the Rhombohedral Setting ($Z = 6$)

centrosymmetric		a = 8.3824 Å		
$R\bar{3}c$ (167)		$\alpha = \beta = \gamma$ = 96.86°		
atom	WP	x	y	z
Ba	6*e*	3/4	0.3902	0.1099
B	12*f*	0.0144	0.1080	0.2356
O(1)	12*f*	0.0100	0.2221	0.1311
O(2)	12*f*	0.9073	0.6655	0.0881
polar−SHG active		a = 8.3824 Å		
$R3c$ (161)		$\alpha = \beta = \gamma$ = 96.86°		
atom	WP	x	y	z
Ba	6*b*	0.3892	0.0333	0.7530
B(1)	6*b*	0.6310	0.7747	0.8560
B(2)	6*b*	0.0586	0.1022	0.8849
O(1)	6*b*	0.6577	0.8751	0.7347
O(2)	6*b*	0.6066	0.2710	0.6854
O(3)	6*b*	0.2921	0.0091	0.4399
O(4)	6*b*	0.1378	0.9725	0.9309

Figure 1b). With the aid of the amplimodes software,[30] we perform the group-theoretical analysis of BaB_2O_4, decomposing it into $M(\tau,m)$ modes. We find that the polar $R3c$ structure is obtained by a single symmetry-unique mode with atomic displacements described by irrep Γ_2^- with a total mode amplitude ($A_{\tau,m}$) of 5.19 Å, which as suggested by Wu et al. provides some insight into the microscopic origin of SHG even in the absence of an explicit calculation of the SHG coefficients.

We further decompose the Γ_2^- distortion mode by Wyckoff positions of the centrosymmetric $R\bar{3}c$ structure, that is, as two M^k modes $M(\Gamma_2^-|e)$ and $M(\Gamma_2^-|f)$ depicted in Figure 1c,d. The former describes displacements of the Ba^{2+} cations atoms in a plane nearly perpendicular to the 3-fold rotation axis, while the latter describes rotations of the anionic $[B_3O_6]^{3-}$ rings about the same 3-fold axis (Figure 1c,d). We find that the greatest contribution to inversion lifting is from the "screw-like" rotation of these borate rings (Table 2), accounting for

Table 2. Normalized Atomic Displacement Patterns e(k) for Each Mode M Decomposed by irrep and Wyckoff Position [(τ,m)|WP] Relative to the Atomic Positions in the Centrosymmetric Reference Phase (Table 1)[a]

	$\Gamma_2^-\|e$	$\Gamma_2^-\|f$
Ba	(0.73, 0.67, 0.13)	
B		(0.74, −0.67, −0.10)
O(1)		(0.96, −0.16, −0.22)
O(2)		(−0.46, 0.88, −0.07)
A_k	0.071	5.187

[a]The decomposition is performed such that the arithmetic centers for the structures are fixed. The amplitude A_k is in units of Å.

~99% of the total distortion connecting the centrosymmetric $R\bar{3}c$ to the polar $R3c$ structure. This structural analysis alone suggests that the borate rings should then make the strongest contribution to the d_{ij} tensor; we investigate this supposition explicitly next through the SAFOR analysis.

We now compute the d_{ij} coefficients for BaB_2O_4 with the $R3c$ fully distorted geometry (FDG, Table 3). According to Kleinmann symmetry[34] and the point group restrictions of $3m$, the SHG d_{ij} tensor has only three independent, nonzero, elements: d_{22}, $d_{31} = d_{15}$, d_{33}. The d_{ij} values we compute with the LDA functional are in good agreement with available experimental data; there is a small underestimation of the magnitude of the experimentally largest coefficient (d_{22}), indicating that our treatment of the electro-optical properties of BaB_2O_4 at the DFT level is sufficient for extracting the atomic structure contribution to the SHG coefficients.

Next, we evaluate d_{ij} by computing $d_{ij}(M_l^k)$ and summing the individual contributions from $M(\Gamma_2^-|e)$ and $M(\Gamma_2^-|f)$. Table 3 shows that linearity is maintained (see the $\sum_l$ column) and that the largest contribution to the SHG response comes from $M(\Gamma_2^-|f)$, corresponding to the rotation of the $[B_3O_6]^{3-}$ rings. In contrast, mode $M(\Gamma_2^-|e)$ makes the largest contribution to the "off-diagonal" ($i \neq j$) SHG coefficients. The small magnitudes found for the d_{31} and d_{33} coefficients show that processes involving different orientations of the polarization plane provide only a minimal contribution to the total response of the material. The negative sign of d_{22} is indicative of a π rotation of the incident light polarization plane about the corresponding crystal axis.

To understand if this result is a consequence in the change in the electronic structure due to the distortions, we compute the electronic density-of-states (DOS) for each mode and compare those results relative to the DOS obtained for the FDG in Figure 2. First, we find an energy gap of about ~4.4 eV. The conduction band and the bottom of the valence band are mainly formed by the O 2*p* and B 2*p* orbitals (atom site and orbital angular momentum decomposed DOS not shown), while the Ba 5*p* states contribute strongly deep in the valence band region near −13.3 eV. Figure 2 shows that the fully distorted structure can be reconstructed by a simple overlap of the single mode contributions owing to the $M(\Gamma_2^-|e)$ and $M(\Gamma_2^-|f)$ displacements, both resembling the global profile of the electronic structure of the FDG. Thus, each geometric distortion's contribution alone to the SHG can be isolated from its induced changes to the electronic structure; the atomic displacement patterns are sufficient to explain the NLO response.

The DOS obtained from the $M(\Gamma_2^-|f)$ distortion strongly resembles that of the equilibrium polar $R3c$ structure. Similar to how this mode alone accounts for much of the d_{22} amplitude, it also effectively generates the electronic structure for which the optical transitions occur between. The rotation of the $[B_3O_6]^{3-}$ rings enables the off-ring oxygen atom with its nonbonding 2*p* states to donate charge to the closest Ba atom under excitation by the electromagnetic field of monochromatic light, because the $M(\Gamma_2^-|f)$ displacements bring the atoms closer together. To confirm this, we perform a computational experiment, where we compute the $d_{ij}(M^k)$ for $M^k = 2 \times M(\Gamma_2^-|f)$, that is, we double the amplitude of the ring displacements relative to the value found in the equilibrium $R3c$ phase. As shown in Table 3, d_{22} is also nearly doubled. We find the charge on the off-ring oxygen atoms is about 6× smaller, obtained by integrating the atom-projected DOS, confirming the enhanced charge transfer toward the closest Ba^{2+} cation. Interestingly, there is a cross-coupling and nonlinear enhancement in the other allowed coefficients: d_{31} increases by a factor of 3 and d_{33} changes sign and increases by an order of magnitude. Understanding such changes in the off-diagonal components from the various atomic displacements requires a more thorough exploration and is currently under investigation. Thus, the SAFOR method is

dx.doi.org/10.1021/ph400049h | ACS Photonics 2014, 1, 96−100

Table 3. Calculated d_{ij} SHG Coefficients in the Static ($\hbar\omega = 0$) Limit for BBO (pm/V) with the Fully Distorted Geometry (FDG, Second Column), Structures Containing Only the $M(\Gamma_2^-|e)$ or $M(\Gamma_2^-|f)$ Modes (Third and Fourth Column), and the Structure Distorted by Doubling the Amplitude of the $\Gamma_2^-|f$ Mode (Third to Last Column)[a]

	calculated						
d_{ij}	FDG	$M(\Gamma_2^-\|e)$	$M(\Gamma_2^-\|f)$	$\sum_l d_{ij}(M_l^k)$	$2 \times M(\Gamma_2^-\|f)$	experiment	ref.
d_{22}	−1.87	−0.029	−1.84	−1.87	−3.49	−2.1 ± 0.1	31
						−2.2 ± 0.2	32
d_{31}	0.030	0.018	0.008	0.026	0.089	0.03	33
d_{33}	−0.028	−0.029	0.009	−0.020	0.39	−0.04	33

[a]Experimental values taken at 1.064 μm. The static approximation is anticipated to be a good reference for the experiments, because of the weakly dispersive behavior of the first-order dielectric susceptibility (and refractive indices) in the 0−2 eV range.

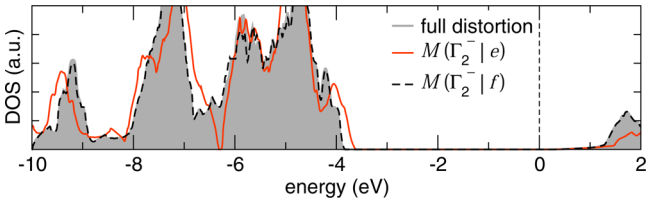

Figure 2. Total density of states (DOS) of the fully distorted (gray shaded region), $M(\Gamma_2^-|e)$ distorted (red, light gray line), and $M(\Gamma_2^-|f)$ distorted (broken black line) structure of BBO. The DOS profile of the fully distorted structure can be seen as simple superposition of the DOS of the Γ_2^- distorted structures.

able to distinguish the dominate displacement patterns promoting second harmonic generation.

Once the distortions responsible of the SHG are individuated, they can be tuned to modulate the NLO response of the material. Our analysis suggests SHG can be enhanced in polar materials by maximizing the density of polar atomic displacements along the unique axis. We conjecture this result is more general and that maximizing *any* noncentrosymmetric distortions, that is, not necessarily polar displacements, could increase the d_{ij} coefficients. Practically, the targeted displacements obtained from the SAFOR identification can be increased through, for example, mechanical constraints, including hydrostatic pressure or epitaxial strain. Indeed, in the former case, increasing pressure in BaB_2O_4 drives the off-ring oxygen atom to shift closer to the Ba^{2+} cation, essentially the $M(\Gamma_2^-|f)$ mode, favoring a transfer of bonding charge from the B−O to the O−Ba bond.[35] In the later thin film geometry, substrate choice and epitaxial constraints with this knowledge can be used to tailor the orientation of the $[B_3O_6]^{3-}$ rings,[36] which influence the SHG performance.[37] We note that, because the SHG performance also depends on the refractive index along different directions in the crystal being similar at the fundamental and doubled-frequencies, that is, the so-called phase matching conditions, enhancing the polar distortions in materials with strong electron−lattice interactions could be detrimental to SHG, as this condition may be attenuated.

In summary, we formulated a general protocol integrating group theory and ab initio electronic structure calculations that is able to elucidate the SHG response in nonlinear optical crystals. This SAFOR approach excludes a priori assumptions on the presence of structural building blocks and atomic polarizability arguments. It provides a symmetry-based explanation of the atomics species, their geometric displacement patterns, and changes to the electronic structure underlying SHG. Moreover, it is not necessary to involve the real-space analysis of the electronic charge density, overcoming the ambiguities and nontrivial search for a reliable partition metric. We tested the method in BaB_2O_4 and established a linear relationship between the polar atomic displacements and the diagonal d_{ij} tensor elements, revealing that the SHG mainly originates from a screw-like rotation of $[B_3O_6]^{3-}$ rings, which enables charge transfer between Ba and oxygen atoms under laser light excitation. Since the SAFOR protocol does not impose any requirements on the crystal topology, we believe the method will be particularly powerful for designing new SHG compounds in diverse material families and chemistries.

AUTHOR INFORMATION

Corresponding Author

*E-mail: jrondinelli@coe.drexel.edu.

Notes

The authors declare no competing financial interest.

ACKNOWLEDGMENTS

A.C. was supported by ONR under Grant No. N00014-11-1-0664. J.M.R. acknowledges the donors of The American Chemical Society Petroleum Research Fund for support (Grant No. 52138-DNI10) and enlightening discussions with K. R. Poeppelmeier, P. Shiv Halasyamani, and S. Pan. This work used the CARBON cluster at the Center for Nanoscale Materials (Argonne National Laboratory) supported by the U.S. DOE, Office of Science, Office of Basic Energy Sciences, under Contract No. DE-AC02-06CH11357. The technical high-performance compute support of Dr. M. Sternberg is gratefully acknowledged, as is the use of the graphical VESTA software.[38]

REFERENCES

(1) Savage, N. Nonlinear crystals. *Nat. Photonics* **2008**, *2*, 380−381.
(2) Guyot-Sionnest, P.; Tadjeddine, A.; Liebsch, A. Electronic distribution and nonlinear optical response at the metal-electrolyte interface. *Phys. Rev. Lett.* **1990**, *64*, 1678−1681.
(3) Steen, W.; Mazumder, J. *Laser Material Processing*, 4th ed.; Springer: London, 2010.
(4) Kissick, D. J.; Wanapun, D.; Simpson, G. J. Second-order nonlinear optical imaging of chiral crystals. *Annu. Rev. Anal. Chem.* **2011**, *4*, 419−437.
(5) Byer, R. L. Nonlinear optical phenomena and materials. *Annu. Rev. Mater. Sci.* **1974**, *4*, 147−190.
(6) Boyd, R. W. *Nonlinear Opt.*, 3rd ed.; Academic Press: San Diego, CA, U.S.A., 2008.
(7) Bordui, P. F.; Fejer, M. M. Inorganic crystals for nonlinear optical frequency conversion. *Annu. Rev. Mater. Sci.* **1993**, *23*, 321−379.
(8) Cyranoski, D. China's crystal cache. *Nature* **2009**, *457*, 953−955.
(9) Chen, C. A localized quantal theoretical treatment, based on an anionic coordination polyhedron model, for EO and SHG effects in crystals of the mixed-oxide type. *Acta Sci. Sin.* **1979**, *22*, 756−776.

(10) Ye, N.; Chen, Q.; Wu, Q.; Chen, C. Searching for new nonlinear optical materials on the basis of the anionic group theory. *J. Appl. Phys.* **1998**, *55*, 555−558.
(11) Song, J.-H.; Freeman, A. J.; Bera, T. K.; Chung, I.; Kanatzidis, M. G. First-principles prediction of an enhanced optical second-harmonic susceptibility of low-dimensional alkali-metal chalcogenides. *Phys. Rev. B* **2009**, *79*, 245203.
(12) Duan, C.-G.; Li, J.; Gu, Z.-Q.; Wang, D.-S. Interpretation of the nonlinear optical susceptibility of borate crystals from first principles. *Phys. Rev. B* **1999**, *59*, 369−372.
(13) Lin, J.; Lee, M.-H.; Liu, Z.-P.; Chen, C.; Pickard, C. J. Mechanism for linear and nonlinear optical effects in β-BaB_2O_4 crystals. *Phys. Rev. B* **1999**, *60*, 13380−13389.
(14) Hu, C. L.; Xu, X.; Sun, C. F.; G., M. J. Electronic structures and optical properties of $Ca_5(BO_3)_3F$: a systematical first-principles study. *J. Appl. Phys.* **2011**, *23*, 395501−395508.
(15) Hu, C.-L.; Mao, J.-G. First-principles study of electronic structures and nonlinear optical properties of $AMoO_3(IO_3)$ (A = Li, Rb and Cs) crystals. *J. Phys.: Condens. Matter* **2010**, *22*, 155801.
(16) Wu, H.; Yu, H.; Yang, Z.; Hou, X.; Su, X.; Pan, S.; Poeppelmeier, K. R.; Rondinelli, J. M. Designing a deep-ultraviolet nonlinear optical material with a large second harmonic generation response. *J. Am. Chem. Soc.* **2013**, *135*, 4215−4218.
(17) Abrahams, S. C.; Kurtz, S. K.; Jamieson, P. B. Atomic displacement relationship to curie temperature and spontaneous polarization in displacive ferroelectrics. *Phys. Rev.* **1968**, *172*, 551−553.
(18) Lin, J.; Lee, M.-H.; Liu, Z.-P.; Chen, C.; Pickard, C. J. Mechanism for linear and nonlinear optical effects in β-BaB_2O_4 crystals. *Phys. Rev. B* **1999**, *60*, 13380−13389.
(19) Eimerl, D.; Davis, L.; Velsko, S.; Graham, E. K.; Zalkin, A. Optical, mechanical, and thermal properties of barium borate. *J. Appl. Phys.* **1987**, *62*, 1968−1983.
(20) Nikogosyan, D. N. Beta barium borate (BBO). *Appl. Phys. A: Mater. Sci. Process.* **1991**, *52*, 359−368.
(21) Perez-Mato, J. M.; Orobengoa, D.; Aroyo, M. I. Mode crystallography of distorted structures. *Acta Crystallogr., Sect. A* **2010**, *66*, 558−590.
(22) Stokes, H. T.; Campbell, B. J.; Cordes, R. Tabulation of irreducible representations of the crystallographic space groups and their superspace extensions. *Acta Crystallogr., Sect. A* **2013**, *69*, 388−395.
(23) Gautier, R.; Norquist, A. J.; Poeppelmeier, K. R. From Racemic Units to Polar Materials. *Cryst. Growth Des.* **2012**, *12*, 6267−6271.
(24) Lines, E.; Glass, A. Principles and applications of ferroelectrics and related materials. *International Series of Monographs on Physics*; Oxford University Press: New York, 1977.
(25) Ceperley, D. M.; Alder, B. J. Ground state of the electron gas by a stochastic method. *Phys. Rev. Lett.* **1980**, *45*, 566−569.
(26) Gonze, X.; et al. ABINIT: First-principles approach to material and nanosystem properties. *Comput. Phys. Commun.* **2009**, *180*, 2582−2615.
(27) Gonze, X. First-principles responses of solids to atomic displacements and homogeneous electric fields: Implementation of a conjugate-gradient algorithm. *Phys. Rev. B* **1997**, *55*, 10337−10354.
(28) Gonze, X.; Lee, C. Dynamical matrices, Born effective charges, dielectric permittivity tensors, and interatomic force constants from density-functional perturbation theory. *Phys. Rev. B* **1997**, *55*, 10355−10368.
(29) Veithen, M.; Gonze, X.; Ghosez, P. Nonlinear optical susceptibilities, Raman efficiencies, and electro-optic tensors from first-principles density functional perturbation theory. *Phys. Rev. B* **2005**, *71*, 125107.
(30) Orobengoa, D.; Capillas, C.; Aroyo, M. I.; Perez-Mato, J. M. *AMPLIMODES*: symmetry-mode analysis on the Bilbao Crystallographic Server. *J. Appl. Crystallogr.* **2009**, *42*, 820−833.
(31) Klein, R.; Kugel, G.; Maillard, A.; Sifi, A.; Polgr, K. Absolute non-linear optical coefficients measurements of BBO single crystal and determination of angular acceptance by second harmonic generation. *Opt. Mater.* **2003**, *22*, 163−169.
(32) Eckardt, R.; Masuda, H.; Fan, Y.; Byer, R. Absolute and relative nonlinear optical coefficients of KDP, KD*P, BaB_2O4, $LiIO_3$, MgO:$LiNbO_3$, and KTP measured by phase-matched second-harmonic generation. *IEEE J. Quant. Electr.* **1990**, *26*, 922−933.
(33) Shoji, I.; Nakamura, H.; Ohdaira, K.; Kondo, T.; Ito, R.; Okamoto, T.; Tatsuki, K.; Kubota, S. Absolute measurement of second-order nonlinear-optical coefficients of β-BaB_2O_4 for visible to ultraviolet second-harmonic wavelengths. *J. Opt. Soc. Am. B* **1999**, *16*, 620−624.
(34) Boulanger, B.; Zyss, J. In *International Tables for Crystallography: Physical Properties of Crystals*; Authier, A., Ed.; International Union of Crystallography: England, 2006; Vol. *D*, pp 176−216
(35) Lu, J. Q.; Lan, G. X.; Li, B.; Yang, Y. Y.; Wang, H. F.; Bai, C. W. Raman scattering study of the single crystal β-BaB_2O_4 under high pressure. *J. Phys. Chem. Solids* **1988**, *49*, 519−527.
(36) Liao, H. B.; Xiao, R. F.; Yu, P.; Wong, G. K. L.; Zheng, J. Q. Preparation of crystalline beta barium borate (β-BaB_2O_4) thin films by opposed-targets magnetron sputtering. *J. Vac. Sci. Technol., A* **1996**, *14*, 2651−2654.
(37) Studebaker, D. B.; Stauf, G. T.; Baum, T. H.; Marks, T. J.; Zhou, H.; Wong, G. K. Second harmonic generation from beta barium borate (β-BaB_2O_4) thin films grown by metalorganic chemical vapor deposition. *Appl. Phys. Lett.* **1997**, *70*, 565−567.
(38) Momma, K.; Izumi, F. *VESTA*: a three-dimensional visualization system for electronic and structural analysis. *J. Appl. Crystallogr.* **2008**, *41*, 653−658.